ENVIRONMENTAL RESEARCH
COMMUNICATIONS

INCLUSIVE PUBLISHING TRUSTED SCIENCE
PURPOSE-LED PUBLISHING™

LETTER • OPEN ACCESS

Remote effect of tropical south Atlantic sea surface temperature anomalies on April–June accumulated cyclone energy over the western North Pacific

To cite this article: Jinjie Song *et al* 2024 *Environ. Res. Commun.* **6** 071007

Environmental Research Communications

LETTER

Remote effect of tropical south Atlantic sea surface temperature anomalies on April–June accumulated cyclone energy over the western North Pacific

Jinjie Song[1,2], **Philip J Klotzbach**[3], **Na Wei**[1] and **Yihong Duan**[2]

[1] Nanjing Joint Institute for Atmospheric Sciences, Chinese Academy of Meteorological Sciences, Nanjing, People's Republic of China
[2] State Key Laboratory of Severe Weather, Chinese Academy of Meteorological Sciences, Beijing, People's Republic of China
[3] Department of Atmospheric Science, Colorado State University, Fort Collins, CO, United States of America

E-mail: songjinjie@qq.com

Keywords: tropical cyclone, accumulated cyclone energy, western North Pacific

OPEN ACCESS

RECEIVED
6 April 2024

REVISED
9 July 2024

ACCEPTED FOR PUBLICATION
12 July 2024

PUBLISHED
24 July 2024

Abstract

Global processes and their teleconnections, such as the El Niño-Southern Oscillation (ENSO), have been shown to be a large driver of interannual changes in accumulated cyclone energy (ACE) of western North Pacific (WNP) tropical cyclones (TCs), with higher ACE during El Niño and lower ACE during La Niña. However, it remains uncertain whether interannual changes in WNP TC ACE are modulated by sea surface temperature anomalies (SSTAs) in other oceans. This study finds a significant negative correlation between WNP TC ACE during the early season (April–June) and simultaneous SSTAs over the tropical south Atlantic (TSA) in 1970–2021. On average, in warm TSA years, basinwide April–June ACE is significantly lower, with significant ACE decreases mainly occurring over the region spanning 5°–30°N, 115°–150°E. This is a result of reduced TC frequency, intensity and duration, due to a remote modulation of WNP environmental conditions by TSA SSTAs. In warm TSA years, there are significant decreases in 700–500-hPa relative humidity, 850-hPa relative vorticity and 200-hPa divergence and significant increases in 850–200-hPa vertical wind shear over the portion of the WNP with significant ACE reductions. These environmental changes can be linked to an anomalous Walker circulation induced by TSA SSTAs.

1. Introduction

Tropical cyclones (TCs) are one of the most destructive and deadliest natural disasters around the world, frequently resulting in large economic losses and casualties for TC-prone coastal regions. Seasonal TC activity can be measured by several commonly used metrics, including the number of TCs with different lifetime maximum intensities (e.g., hurricanes/typhoons) as well as accumulated cyclone energy (ACE; Bell *et al* 2000). ACE is defined as the sum of the squares of 6-hourly maximum sustained wind speeds where a TC is at least of tropical storm intensity ($\geqslant$34 kt). Consequently, ACE serves as an integrated parameter comprising the frequency, intensity and duration of TCs. ACE has been widely used in previous studies to examine historical TC activity as modulated by different climate modes and to project possible TC-related changes in different global warming scenarios (Emanuel 2018).

The western North Pacific (WNP) is the most TC-active basin worldwide, with approximately one-third of global TCs and about 40% of global ACE on an annually-averaged basis (Maue 2011, Lee *et al* 2012). On interannual timescales, El Niño-Southern Oscillation (ENSO) has been shown to be a significant driver of WNP ACE variability. Camargo and Sobel (2005) reported a significant positive correlation between WNP ACE during July–October and simultaneous ENSO indices. In El Niño (La Niña) years, WNP TCs generally formed more southeastward (northwestward), tending to have longer (shorter) lifetimes, attaining higher (lower) intensities, and resulting in greater (lesser) ACE. Furthermore, Patricola *et al* (2018) and Choi *et al* (2019) noted that relative

to neutral ENSO events, central Pacific (CP) El Niño events exhibited greater ACE increases than eastern Pacific (EP) El Niño events, when considering sea surface temperature (SST) anomalies (SSTAs) with the same magnitudes over the CP and EP.

In addition to ENSO, several studies have found other factors influencing interannual changes in WNP ACE. Zhan and Wang (2016) showed that in years with a positive zonal component of vertical wind shear (VWS) over the equatorial WNP or a positive SST gradient between the southwestern Pacific and the western Pacific warm pool, WNP TCs during June–October tended to be weaker and shorter lived, resulting in less ACE. Song *et al* (2022) found a significant inverse relationship between WNP ACE during July–October and the simultaneous Pacific-North American (PNA) pattern, with greater (lesser) basinwide ACE in positive (negative) PNA years. Additionally, Patricola *et al* (2022) reported that greater (lesser) WNP ACE during May–November was significantly linked to a positive (negative) phase of the Atlantic Meridional Mode.

All of the aforementioned findings focused on ACE changes during the peak or full WNP TC season. Other research has noted a distinct seasonal relationship between WNP ACE and climate modes (e.g., Wang *et al* 2013, Choi *et al* 2019). For example, Wang *et al* (2013) found that during the early season from April–June (AMJ), ENSO had only a minor impact on TC number, lifetime and intensity, resulting in a weak relationship between ENSO and early-season WNP ACE. This result was likely due to ENSO-related SSTAs during AMJ being relatively small, as ENSO events are often initiating during this season. By comparison, ENSO's impact on WNP ACE gradually increases with the development of ENSO events, with significant ENSO-induced changes in WNP TC ACE occurring particularly during the peak season from July–September and the late season from October–December (Wang *et al* 2013, Choi *et al* 2019).

Until now, there has been little research on what controls interannual changes in WNP ACE during the early season. Figure 1(a) shows that the largest region with significant correlations between WNP ACE and SSTAs during AMJ occurs over the tropical south Atlantic (TSA). Recently, some studies (e.g., Yang *et al* 2023, Sheng *et al* 2023, Zhang *et al* 2023) reported a remote interannual modulation of environmental changes over East Asia by TSA SSTAs. During boreal springs with positive TSA SSTAs, East Asian surface air temperatures were cooler, the Meiyu onset was earlier, and the WNP anticyclone was stronger.

Accordingly, the objective of this work is to examine the interannual linkage between early-season WNP ACE and simultaneous TSA SSTAs, as well as its potential large-scale driving mechanisms. Section 2 introduces the data used in this study. Section 3 documents changes in WNP TC activity as modulated by TSA SSTAs, while section 4 looks at changes in environmental conditions as modulated by TSA SSTAs. Section 5 discusses the robustness of our proposed mechanism. Section 6 concludes with a summary.

2. Data and methods

This study uses 6-hourly TC best track data for 1970–2021 from the Joint Typhoon Warning Center as compiled by the International Best Track Archive for Climate Stewardship (IBTrACS) (v04r00; Knapp *et al* 2010), including TC central position and 1-min maximum sustained wind speed over the WNP (north of the equator and 100°E–180°). Data prior to 1970 are not evaluated, owing to larger uncertainties in TC intensity estimation (Emanuel 2000, Camargo and Sobel 2005). There have been several publications (e.g., Emanuel 2000, Camargo and Sobel 2005, Maue 2011, Wu *et al* 2020, Wang and Li 2022) investigating changes in WNP TC ACE on seasonal-to-decadal timescales using TC best track data since 1970. Thus, we retain data from 1970–2021 to expand our sample size without diminishing the quality of the data. Our results are not significantly changed if we use a shorter period with higher quality data from 1980–2021 (figures not shown). Given that tropical depressions are excluded in the computation of ACE (Bell *et al* 2000) and also exhibited large detection uncertainty due to changing observational techniques (Klotzbach and Landsea 2015), only records when TCs are of at least tropical storm intensity ($\geqslant$34 kt) are taken into consideration. As previously noted, this study focuses on WNP ACE during the early season of AMJ, which accounts for ~11% of annual WNP ACE. There are a total of 190 WNP TCs that formed during AMJ from 1970 to 2021 met these criteria.

TC genesis is identified as the first record in the best track data, while TC genesis density is obtained by counting the frequency of TC formations on individual $5^\circ \times 5^\circ$ grids. Similarly, TC track density is derived as the occurrence frequency of 6-h TC records in each $5^\circ \times 5^\circ$ box, while gridded ACE and average intensity are calculated over the same box.

Monthly mean SST data on a $1^\circ \times 1^\circ$ grid are taken from the Hadley Centre Sea Ice and Sea Surface Temperature data set (HadISST; Rayner *et al* 2003). Monthly mean atmospheric variables are derived from the fifth generation European Centre for Medium-Range Weather Forecasts (ECMWF) reanalysis of the global climate (ERA5; Hersbach *et al* 2020), with a resolution of $0.25^\circ \times 0.25^\circ$. These datasets are used to calculate thermodynamic and dynamic variables influencing TC activity, such as SST, maximum potential intensity (MPI;

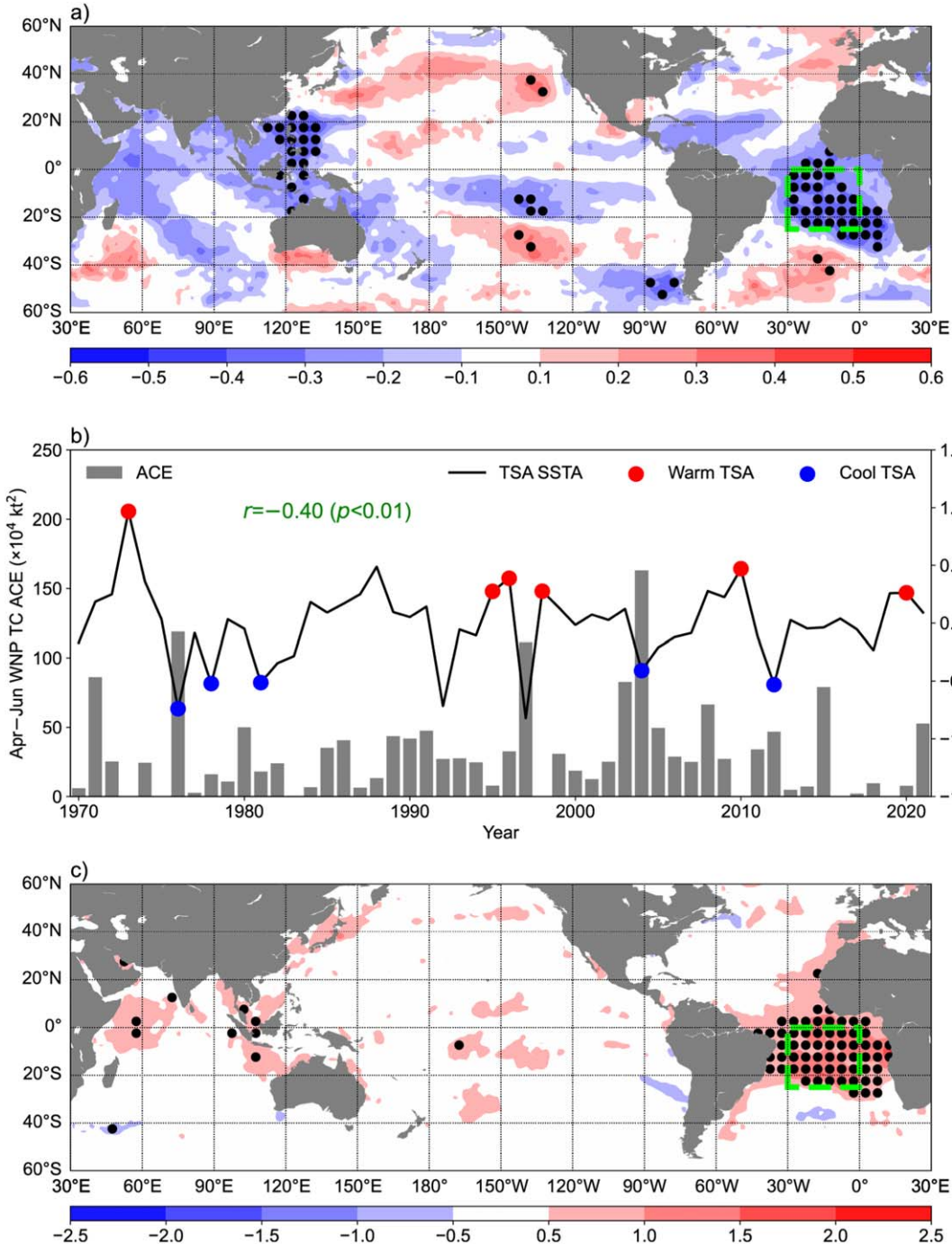

Figure 1. (a) Spatial distribution of the correlation between western North Pacific (WNP) accumulated cyclone energy (ACE) during April–June (AMJ) and simultaneous sea surface temperature (SST) anomalies (SSTAs) from 1970 to 2021. Black dots denote correlations significant at the 0.05 level. The green box denotes the tropical South Atlantic (TSA) region. (b) Annual variation of WNP ACE and TSA SSTA during AMJ from 1970 to 2021. Correlation coefficients and significance levels are shown in the panel. Red and blue dots refer to warm and cool TSA years, respectively. These years were identified by excluding El Niño-Southern Oscillation (ENSO). (c) Differences in SST (°C) between warm and cool TSA years. Black dots denote differences significant at the 0.05 level. The green box denotes the TSA region.

Emanuel 1988), 700–500-hPa relative humidity, 850-hPa relative vorticity, 200-hPa divergence and 850–200-hPa VWS.

The SSTA indices over different regions, e.g., the Niño-3.4 region (5°S–5°N, 170°–120°W), the TSA (25°S–0°, 30°W–0°) and the Philippine Sea (PS; 0°–20°N, 120°–140°E), are all calculated from detrended SST fields. Given a significant inverse correlation between Niño-3.4 and TSA SSTAs ($r = -0.32$; $p = 0.02$), warm and cool TSA years are classified using a ±0.8 standard deviation threshold for the TSA SSTA index, while excluding El Niño and La Niña years with a magnitude of the Niño-3.4 SSTA index greater than 0.8 standard deviations. This threshold of 0.8 standard deviation has been used to select years in previous TC-related studies (e.g., Zhan

et al 2011, Zhao *et al* 2023, Shi *et al* 2024). Our results remain relatively unchanged, if other thresholds (e.g., 0.6 or 1 standard deviation) are used (tables not shown). Using this classification approach, we obtain six warm TSA years (1973, 1995, 1996, 1998, 2010 and 2020) and five cool TSA years (1976, 1978, 1981, 2004 and 2012).

In order to confirm these results, we examined climate model simulations using the medium-resolution version of the Beijing Climate Center (BCC) Climate System Model (BCC-CSM2-MR), serving as the baseline for BCC's participation in the Coupled Model Intercomparison Project Phase 6 (CMIP6). BCC-CSM2-MR was run at a horizontal resolution of spectral triangular 106 (T106) in the atmosphere and 1° latitude × 1° longitude in the ocean, while its other configurations can be found in Wu *et al* (2021).

The significance levels (p) of correlation coefficients (r), partial correlation coefficients, pattern correlation coefficients and differences in means between two samples are estimated by using a two-tailed Student's t-test. The significance levels of regressions and partial regressions are estimated through an F-test. When evaluating statistical significance, the effective sample size proposed in Trenberth (1984) was applied to minimize the influence of autocorrelation.

3. The influence of TSA SSTAs on TC activity

Figure 1(a) displays the spatial pattern of correlation coefficients between basinwide ACE over the WNP and near-global SSTAs during AMJ from 1970 to 2021. Consistent with Wang *et al* (2013), correlations are low over the equatorial central-to-eastern Pacific, confirming a weak ACE-ENSO relationship during the early season ($r = -0.02$; $p = 0.91$). Significant negative correlations do occur, however, over the TSA and PS. Although the correlations of basinwide ACE versus TSA SSTA ($r = -0.40$; $p < 0.01$; figure 1(b)) and PS SSTA ($r = -0.31$; $p = 0.02$) are not strong, both of them are statistically significant. When excluding the impact of PS SSTA, the partial correlation between ACE and TSA SSTA remains significant ($r = -0.35$; $p = 0.01$). When excluding ENSO's impact, the partial correlation between ACE and TSA SSTA remains almost unchanged ($r = -0.40$; $p < 0.01$). These results imply that the impact of TSA SSTA on WNP ACE is independent of the impacts of PS SSTA and ENSO. By comparison, when removing the impact of TSA SSTA, the partial correlation between ACE and PS SSTA does weaken somewhat ($r = -0.25$; $p = 0.07$). These results mean TSA SSTA and PS SSTA can explain 12% and 6% of the variance in interannual ACE changes, respectively, when controlling for the other region.

Figure 1(c) shows SST differences between warm and cool TSA years. Significant differences are concentrated over the TSA, with SST anomalies generally of a small magnitude over the remainder of the global ocean. Particularly, there are no significant SST differences over almost the entire Pacific. This means that TSA SSTA has only a minor impact on WNP SST, which is consistent with a weak correlation between TSA and PS SSTAs ($r = 0.20$; $p = 0.16$).

Figure 2 displays the regressions and partial regressions of WNP ACE onto TSA SSTA and PS SSTA during 1970–2021. Although there are both basinwide reductions in ACE over the WNP induced by TSA SSTA and PS SSTA, the regions with significant ACE changes are not completely coincident. Significant TSA SSTA-induced ACE decreases are observed over the region of 5°–35°N, 120°–155°E (figure 2(a), (c)), while significant PS SSTA-induced ACE decreases are concentrated over two regions spanning 10°–20°N, 115°–125°E and 5°–25°N, 140°–160°E (figures 2(b), (d)). The spatial patterns of TSA SSTA-induced and PS SSTA-induced ACE changes look like reductions in recurving and straight-moving TCs over the WNP, respectively. These results mean that ACE changes modulated by TSA SSTA are likely to be different from those modulated by local SSTAs.

On average, basinwide ACE over the WNP is 20×10^4 kt^2 in warm TSA years and 140×10^4 kt^2 in cool TSA years, with WNP ACE being significantly lower in warm TSA years than in cool TSA years (table 1). Table 1 also shows differences in some of the metrics contributing to ACE between warm and cool TSA years. Generally speaking, in warm TSA years, there are fewer TCs with shorter lifetimes over the WNP, resulting in fewer TC days. TC days are defined as the total number of days where there are TCs of at least tropical storm intensity. This metric is calculated by summing the number of 6-h periods when TCs occur. In addition, the average intensity of WNP TCs is lower in warm TSA years. These findings show that in warm TSA years, WNP TC activity during AMJ is significantly suppressed, regardless of whether examining storm frequency, intensity or duration. Table 2 shows that the correlations of TC number versus ACE and TSA SSTAs are both the highest among the four ACE-related TC parameters. It is likely that TSA SSTA modulates ACE primarily through its influence on TC frequency.

Figure 3 presents the spatial distributions of the differences in ACE-related metrics during AMJ between warm and cool TSA years. In warm TSA years, ACE is suppressed across most of the WNP, with the maximum ACE decreases occurring east of the Philippines (figure 3(a)). Significant ACE reductions occurred in the region spanning 5°–30°N, 115°–150°E, while there are almost no changes in ACE east of 160°E. Other TC metrics showed similar near-basinwide reductions in warm TSA years (figures 3(b)–(d)). TC genesis was suppressed

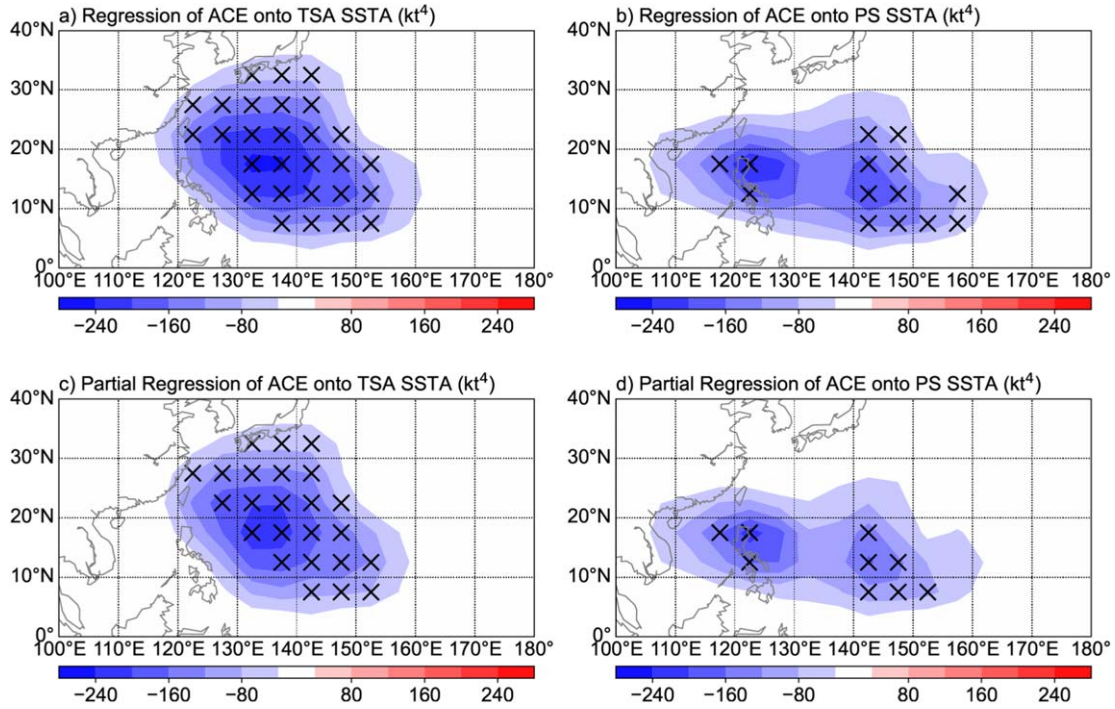

Figure 2. (a), (b) Regressions and (c), (d) partial regressions of western North Pacific accumulated cyclone energy (ACE) onto the normalized (a), (c) tropical South Atlantic (TSA) sea surface temperature anomaly (SSTA) and (b), (d) Philippine Sea (PS) SSTA during April–June from 1970 to 2021. Black crosses refer to regressions significant at the 0.05 level.

Table 1. WNP TC metrics during AMJ averaged over six warm TSA years and five cool TSA years, as well as their differences and the corresponding significance levels.

	Warm TSA	Cool TSA	Difference
ACE ($\times 10^4$ kt^2)	20	140	−120 ($p = 0.04$)
TC Number	1.7	6.0	−4.3 ($p < 0.01$)
Average Lifetime (h)	77.8	256.0	−178.2 ($p = 0.03$)
TC Days	11.5	67.5	−56.0 ($p = 0.02$)
Average Intensity (kt)	44.2	62.2	−18.0 ($p = 0.04$)

Table 2. Correlations of WNP TC metrics with ACE and TSA SSTAs during AMJ from 1970 to 2021, as well as their corresponding significance levels.

	Correlation with ACE	Correlation with TSA SSTA
TC Number	0.95 ($p < 0.01$)	−0.42 ($p < 0.01$)
Average Lifetime (h)	0.57 ($p < 0.01$)	−0.38 ($p < 0.01$)
TC Days	0.75 ($p < 0.01$)	−0.34 ($p < 0.01$)
Average Intensity (kt)	0.76 ($p < 0.01$)	−0.41 ($p < 0.01$)

west of 160°E, with significant decreases in genesis density occurring near 130°E and 150°E (figure 3(b)). As a result, TC track densities also decreased over most of the WNP, with significant decreases over two sub-regions: 15°–30°N, 110°–135°E and 5°–25°N, 140°–155°E (figure 3(c)). These TC occurrence decreases over the western and eastern sub-regions can be linked to TC genesis reductions near 130°E and 150°E, respectively. In addition, average TC intensity significantly decreases over the region spanning 5°–35°N, 110°–155°E, which is somewhat larger than the region with significant TC track density decreases (figure 3(d)). The spatial structures of the differences in TC track density and average intensity both exhibit a high similarity to that for ACE (figures 3(a),

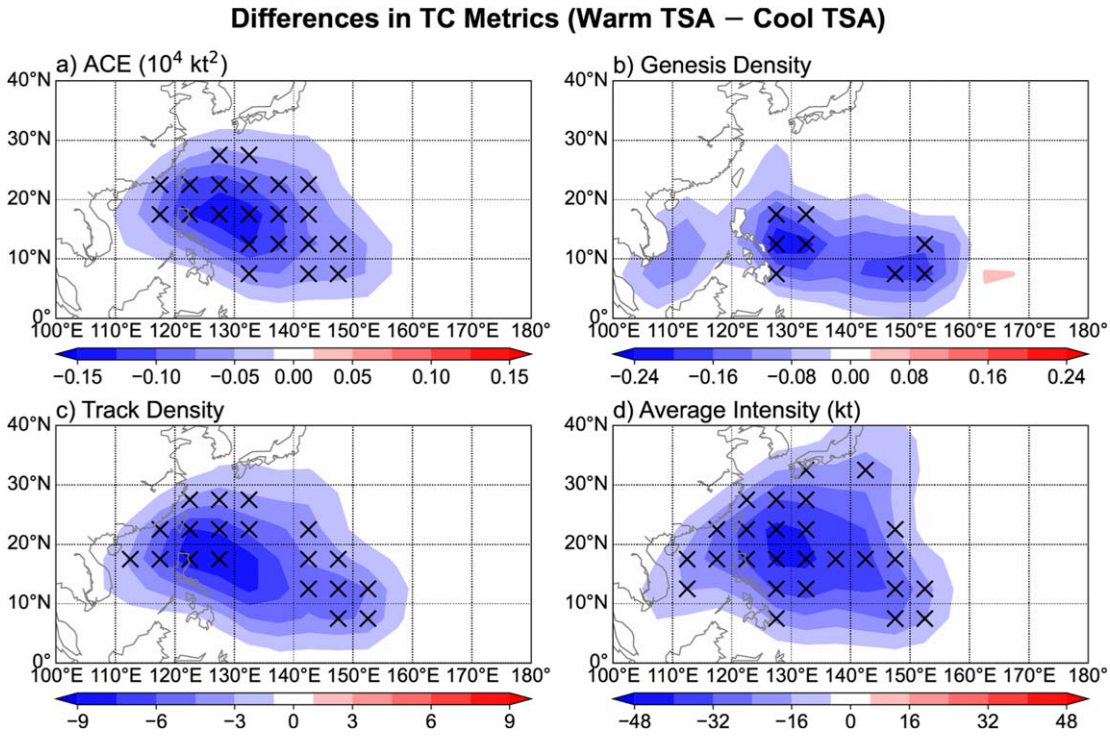

Figure 3. Differences in (a) accumulated cyclone energy (ACE), (b) genesis density, (c) track density and (d) average intensity of western North Pacific tropical cyclones during April–June between warm and cool tropical South Atlantic (TSA) years. All TC metrics are counted in a 5° latitude × 5° longitude horizontal box. Black crosses refer to differences significant at the 0.05 level.

(c), (d)), with pattern correlation coefficients of 0.99 ($p < 0.01$) and 0.94 ($p < 0.01$), respectively. These results confirm that in warm TSA years, decreases in TC occurrence and intensity both favor reductions in ACE.

4. The influence of TSA SSTAs on environmental conditions

Changes in environmental conditions play a dominant role in influencing TC activity on interannual timescales (Walsh *et al* 2016). As noted in Wang and Zhou (2008), similar environmental characteristics favor both TC genesis and intensification. Figure 4 shows differences in environmental conditions over the WNP during AMJ between different TSA years. In warm TSA years, SST and MPI changes exhibit similar patterns, with increased SSTs and MPIs extending from the South China Sea (SCS) northeastward to the subtropical WNP and eastward to the equatorial central Pacific (figures 4(a), (b)). This similarity is due to SST playing an important role in estimating MPI (Emanuel 1988). However, there are almost no significant SST and MPI changes over the basin, indicating that TSA SSTA likely play only a minor role in modifying WNP oceanic conditions.

By contrast, TSA anomalies do cause significant differences in the WNP atmospheric circulation (figures 4(c)–(f)). In warm TSA years, there are significant decreases in both 700–500-hPa relative humidity and 200-hPa divergence within the latitudinal belt of 10°–20°N, with only weak increases north of 25°N (figures 4(c), (e)). Significant decreases in 850-hPa relative vorticity occur over a broader latitudinal belt of 10°–30°N (figure 4(d)). There are significant increases in 850–200-hPa VWS extending from the northwestern WNP to the southeastern WNP, with significant VWS decreases concentrated over the southwestern WNP (figure 4(f)).

In warm TSA years, changes in the four atmospheric variables that we examined all suppressed TC genesis near 130°E and 150°E, including significantly reduced humidity, low-level vorticity and upper-level divergence and significantly enhanced VWS (figures 4(c)–(f)). The region in between the two regions with suppressed TC genesis (centered near 140°W) showed insignificant changes for humidity, divergence, vorticity and VWS, likely explaining the lack of TC genesis changes in this region. The spatial distribution of TC genesis changes is well captured by changes in humidity, vorticity, divergence and VWS, with significant pattern correlation coefficients of 0.31 ($p < 0.01$), 0.33 ($p < 0.01$), 0.30 ($p < 0.01$) and −0.17 ($p < 0.01$), respectively. The correlations between areal averaged environmental variables and TC genesis over the region of 135°–145°E are much weaker than over the region of 25°–135°E and 145°–155°E (tables not shown). This implies that TC genesis is less sensitive to environmental changes between 135°E and 145°E, leading to geographical separation of observed TC genesis reductions.

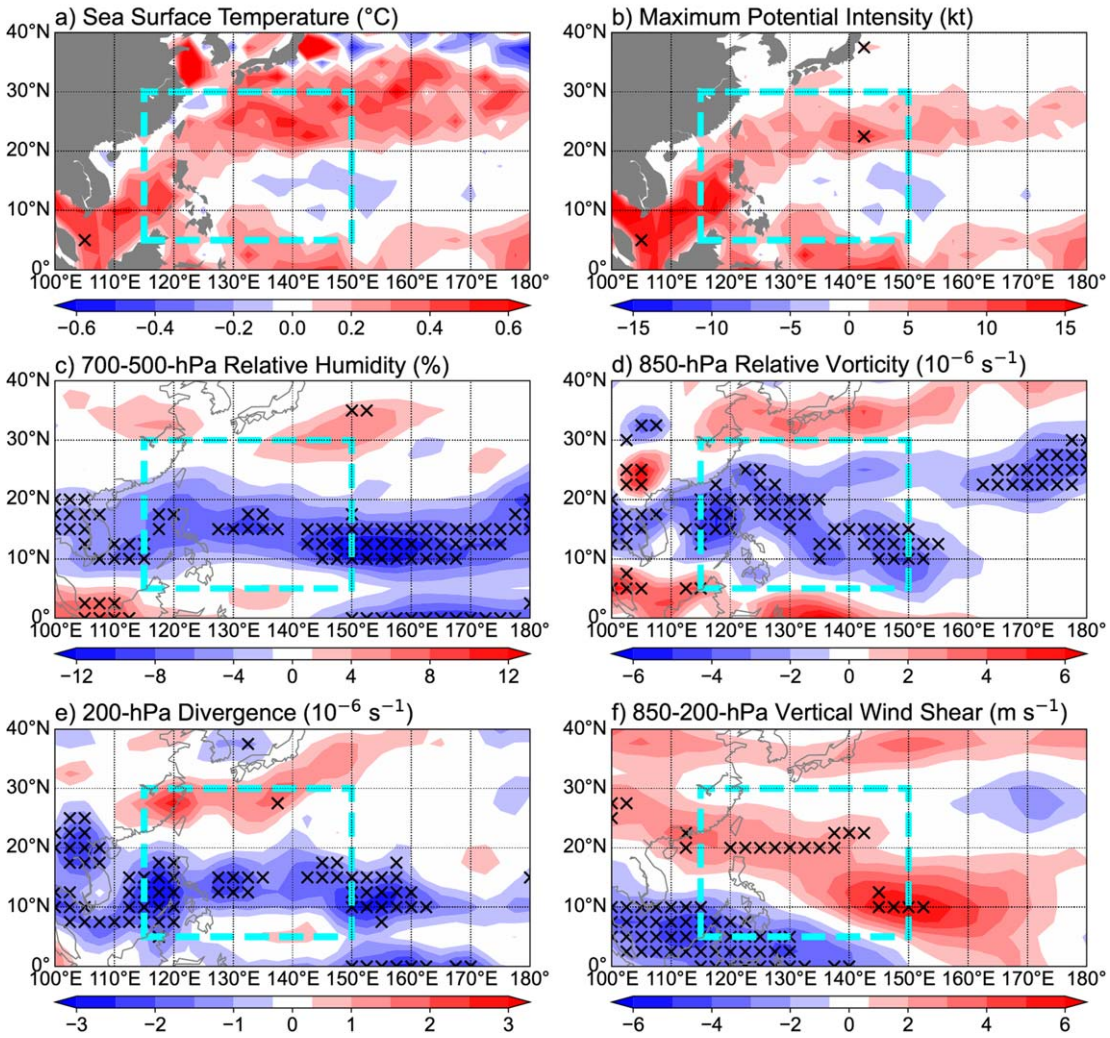

Figure 4. Differences in (a) sea surface temperature, (b) maximum potential intensity, (c) 700–500-hPa relative humidity, (d) 850-hPa relative vorticity, (e) 200-hPa divergence and (f) 850–200-hPa vertical wind shear during April–June between warm and cool tropical South Atlantic (TSA) years. Black crosses refer to differences significant at the 0.05 level. Cyan boxes denote the region with significant accumulated cyclone energy changes between warm and cool TSA years (5°–30°N and 115°–150°E).

Because of the aforementioned unfavorable atmospheric changes south of 30°N, TC intensification is suppressed and TC intensity is on average lower in warm TSA years. In addition, there are also significant decreases in average TC intensity north of 30°N (figure 3(d)), which is not simply explained by environmental conditions in the mid-latitudes. Mid-latitude environmental conditions show little change in warm TSA years (figure 4). Instead, given the suppression of TC intensification over the tropical WNP, TCs tend to attain a relatively lower lifetime maximum intensity in warm TSA years (table 1). When moving northward into higher latitudes, these TCs weaken and consequently have lower intensities than in cool SSTA years.

Figure 5 examines how TSA SSTAs affect TC-related environmental conditions over the WNP through atmospheric circulation modulations. In warm TSA years, positive SSTAs over the TSA can trigger locally enhanced convection associated with anomalous upward motion between 60°W–0° (figure 5). There is an anomalous Walker circulation that reaches from the equatorial Atlantic to the equatorial central Pacific, with associated anomalous westerlies and easterlies at lower and upper levels, respectively (figure 5(a)). Correspondingly, significant descending anomalies occur over the equatorial eastern WNP (150°E–180°) with associated reduced convection as demonstrated by increased outgoing longwave radiation (OLR) (figures 5(b), (c)).

In warm TSA years, as a result of this decreased convective activity and increased diabatic cooling that peaks between 150°–170°E near the equator (figure 5(c)), there is an anomalous low-level anticyclonic circulation to its northwest due to a Matsuno-Gill response (Matsuno 1966, Gill 1980). This response is centered at around 20°N, 150°E but covers almost the entire WNP (figure 5(b)). This anomalous anticyclone is associated with

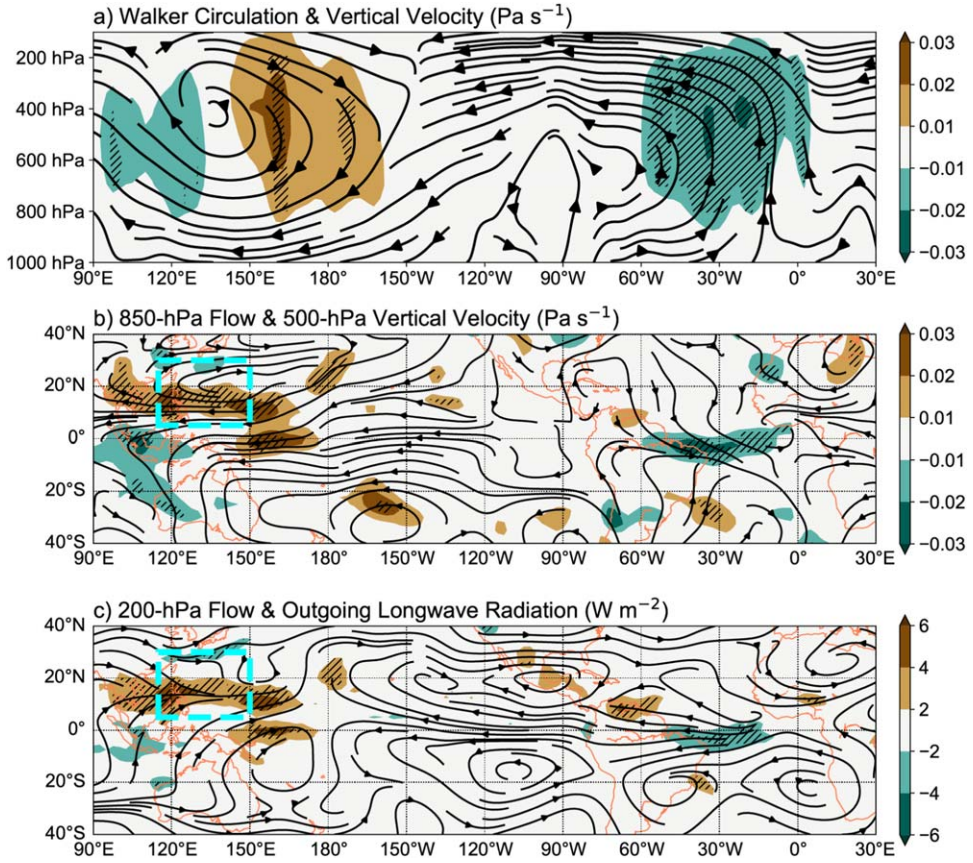

Figure 5. (a) Differences in the Walker circulation and vertical velocity averaged within 10°S–10°N between warm and cool tropical South Atlantic (TSA) years. Streamlines are plotted after multiplying vertical velocity differences by 1000 at each pressure level. Vertical velocity differences significant at the 0.05 level are hatched. (b) Differences in 850-hPa flow and 500-hPa vertical velocity between warm and cool TSA years. Vertical velocity differences significant at the 0.05 level are hatched. (c) Differences in 200-hPa flow and outgoing longwave radiation (OLR) between warm and cool TSA years. OLR differences significant at the 0.05 level are hatched. Cyan boxes denote the region with significant accumulated cyclone energy changes between warm and cool TSA years (5°–30°N and 115°–150°E).

anomalous descending motion based on quasi-geostrophic theory (figure 5(b)). This anticyclone inhibits upward moisture transport from the underlying ocean surface and subsequently reduces atmospheric humidity. This anomalous anticyclone also produces negative low-level vorticity anomalies, suppressing basinwide TC activity over the WNP.

In addition, over the latitudinal belt spanning 5°–20°N, the aforementioned downdrafts and low-level anticyclonic circulation both correspond to upper-level convergent flow, rather than a cyclonic circulation (figure 5(c)). Climatologically, there are low-level easterlies and upper-level westerlies over most of the WNP, except for the SCS (figure 6). Over the region of 5°–30°N, 115°–150°E, in warm TSA years, the anomalous low-level easterlies and upper-level westerlies are in the same directions as their corresponding climatological flows (figures 5(b), (c)), inducing increased VWS.

5. Discussion

To confirm the remote influence of TSA SSTA on environmental changes over the WNP, we designed idealized numerical simulations using the BCC-CSM2-MR model forced by different SSTAs over the TSA. The control run was integrated for 50 years, driven by climatological AMJ SST based on the period of 1970–2021. Two sensitivity runs were forced by adding 0.15°C and 0.30°C to SSTs over the TSA, which roughly corresponded to 0.5 standard deviations and 1 standard deviation of the annual TSA SSTA series. The anomalous fields were then derived as the differences between the sensitivity runs and the control run.

Figure 7 presents the simulated 850-hPa anomalous flow over the WNP driven by TSA SSTA. Consistent with the differences in the observed flow between warm and cool TSA years, there is an anomalous low-level large-scale anticyclone over the WNP in the simulation, centered at around 15°N, 150°E, regardless of if the 0.15°C or 0.30°C TSA SSTA forcing are used. The strength of this simulated anomalous anticyclone increases

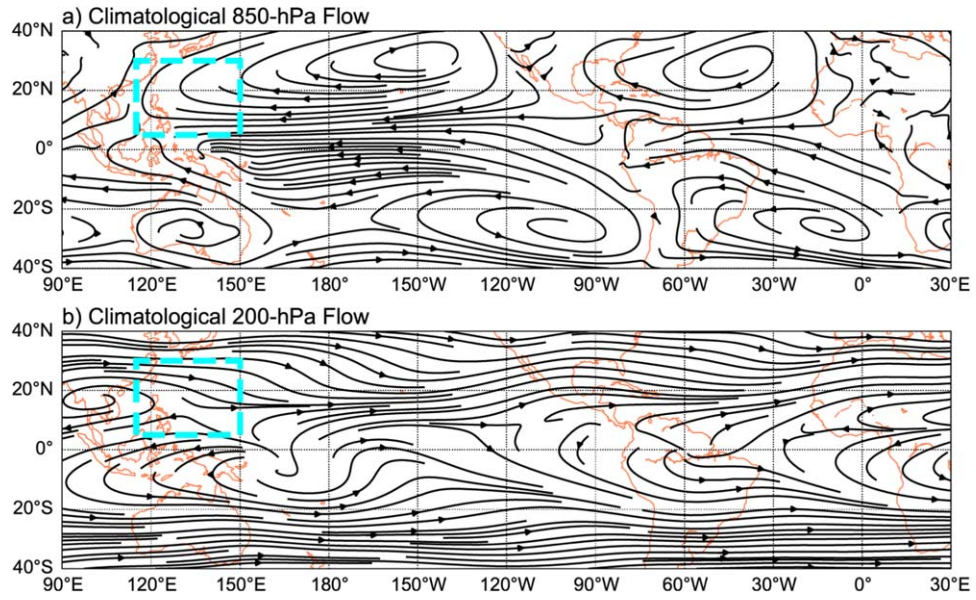

Figure 6. Climatological (a) 850-hPa and (b) 200-hPa horizontal flow during April–June between 1970 and 2021. Cyan boxes denote the region with significant accumulated cyclone energy changes between warm and cool TSA years (5°–30°N and 115°–150°E).

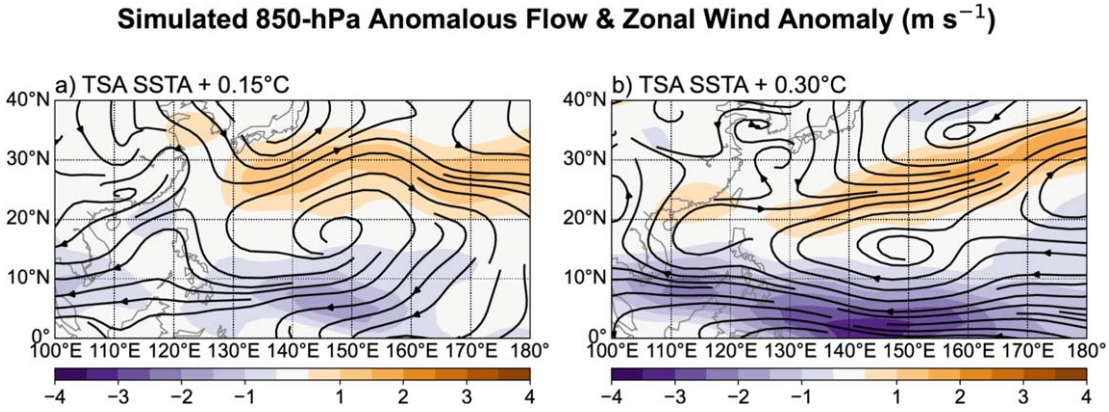

Figure 7. Simulated 850-hPa anomalous flow and zonal wind anomaly for the experiments driven by a (a) tropical South Atlantic (TSA) sea surface temperature anomaly (SSTA) of +0.15°C and (b) TSA SSTA of +0.30°C.

with TSA SSTA, corresponding to increased low-level easterlies to the south of the anticyclone and increased low-level westerlies to the north of the anticyclone. These results confirm that TSA SSTA can remotely induce changes in the WNP atmospheric circulation.

6. Summary

The interannual variability of WNP ACE during the early season is investigated in this study. There is a significant correlation between early-season (April–June) ACE over the WNP and mean SSTA over the TSA from 1970–2021. On average, basinwide ACE is significantly lower in warm TSA years than in cool TSA years. In warm TSA years, there are significant ACE decreases over the region of 5°–30°N, 115°–150°E and weak ACE changes east of 160°E. This is induced by a suppression of TC activity over most of the WNP, including reduced TC genesis, decreased TC occurrence as well as weakened TC intensity. The significant decrease in TC number appears to be the most important factor leading to ACE reductions in warm TSA years.

The remote influence of TSA SSTA on ACE can be explained by changes in large-scale WNP environmental variables. There are almost no significant changes in the oceanic variables investigated: SST and MPI. However, there are significant differences in atmospheric variables between different TSA years. In warm TSA years, there are significant decreases in 700–500-hPa relative humidity and 200-hPa divergence within the latitudinal belt of

10°–20°N, while significant decreases in 850-hPa relative vorticity occur over a broader latitudinal belt of 10°–30°N. In addition, there are significant increases in 850–200-hPa VWS extending from the northwestern WNP to the southeastern WNP. Changes in these four atmospheric variables all suppress both WNP TC genesis and TC intensity. These results also imply that TSA SSTA can influence WNP TC activity primarily through modulating WNP atmospheric conditions.

In warm TSA years, positive SSTAs over the TSA can trigger locally enhanced convection that is associated with an anomalous Walker circulation spanning from the equatorial Atlantic to the equatorial central Pacific. The descending branch of this anomalous Walker circulation is centered near the equator and from 150°–170°E, causing reduced convective activity and enhanced diabatic cooling. The associated Matsuno-Gill response results in an anomalous large-scale low-level anticyclone over the WNP, causing negative vorticity anomalies. This anticyclone is also associated with anomalous sinking motion, inhibiting upward moisture transport from the underlying ocean. In warm TSA years, the anomalous low-level easterlies and upper-level westerlies over most of the WNP are in the same directions as their corresponding climatological flow, leading to increased VWSs.

Previous studies (e.g., Wu *et al* 2017a, Wu *et al* 2017b, Li *et al* 2018) suggested that local SSTAs could trigger and maintain an anomalous WNP anticyclone (WNPAC), suppressing WNP TC activity. Warm PS SSTA can generate local anomalous convection, resulting in an anomalous anticyclonic low-level circulation to its northeast through a Matsuno-Gill response. By comparison, warm TSA SSTA can induce an anomalous Walker cell with anomalous descending motion between 150°E and 170°E, leading to an anomalous anticyclonic low-level circulation to its northwest through a Matsuno-Gill response. These imply that TSA and PS SSTAs induce similar changes in the low-level circulation through different pathways.

Our results highlight a remote modulation of WNP TC activity during the early season by SSTAs in the Western and Southern Hemispheres. Our findings can be utilized as a potential predictor for seasonal TC forecasting, resulting in improved early season skill. One caveat of our research is that our results are obtained from a statistical analysis of a limited number of samples. Our main findings will be verified in future work using additional numerical experiments and different SSTA forcings over the TSA.

Acknowledgments

The authors would like to express their sincere thanks to three anonymous reviewers for their helpful comments on an earlier version of this manuscript. This work was jointly funded by the National Natural Science Foundation of China: U2342203, 61827901, 42175007, 41905001 and 4219255; G. Unger Vetlesen Foundation; Meteorological Research Program of Guangxi Province of China.

Data availability statement

The data cannot be made publicly available upon publication because they are not available in a format that is sufficiently accessible or reusable by other researchers. The data that support the findings of this study are available upon reasonable request from the authors.

ORCID iDs

Jinjie Song https://orcid.org/0000-0003-3948-8894
Na Wei https://orcid.org/0000-0002-5541-6068

References

Bell G D, Halpert M S, Schnell R C, Higgins R W, Lawrimore J, Kousky V E, Tinker R, Thiaw W, Chelliah M and Artusa A 2000 Climate assessment for 1999 *Bull. Am. Meteorol. Soc.* **81** 1328–1328
Camargo S J and Sobel A H 2005 Western North Pacific tropical cyclone intensity and ENSO *J. Clim.* **18** 2996–3006
Choi Y, Ha K and Jin F 2019 Seasonality and El Niño diversity in the relationship between ENSO and western North Pacific tropical cyclone activity. *J. Clim.* **32** 8021–45
Emanuel K A 1988 The maximum intensity of hurricanes *J. Atmos. Sci.* **45** 1143–55
Emanuel K A 2000 A statistical analysis of tropical cyclone intensity *Mon. Weather Rev.* **128** 1139–52
Emanuel K A 2018 100 years of progress in tropical cyclone research *Meteorological Monographs* **59** 1–68
Gill A E 1980 Some simple solutions for heat-induced tropical circulation *Q. J. R. Meteorolog. Soc.* **106** 447–62
Hersbach H *et al* 2020 The ERA5 global reanalysis *Q. J. R. Meteorolog. Soc.* **146** 1999–2049
Klotzbach P J and Landsea C W 2015 Extremely intense hurricanes: revisiting Webster *et al* (2005) after 10 years *J. Clim.* **28** 7621–9
Knapp K R, Kruk M C, Levinson D H, Diamond H J and Neumann C J 2010 The international best track archive for climate stewardship (IBTrACS) unifying tropical cyclone data *Bull. Am. Meteorol. Soc.* **91** 363–76

Lee T –C, Knutson T R, Kamahori H and Ying M 2012 Impacts of climate change on tropical cyclones in the western North Pacific basin. Part I: past observations *Tropical Cyclone Research and Review* **1** 213–30
Li T, Wang B, Wu B, Zhou T, Chang C –P and Zhang R 2018 Theories on formation of an anomalous anticyclone in western North Pacific during El Niño: a review. *Journal of Meteorological Research* **31** 987–1006
Matsuno T 1966 Quasi-geostrophic motions in the equatorial area *Journal of the Meteorological Society of Japan* **44** 25–43
Maue R N 2011 Recent historically low global tropical cyclone activity *Geophys. Res. Lett.* **38** L14803
Patricola C M, Camargo S J, Klotzbach P J, Saravanan R and Chang P 2018 The influence of ENSO flavors on western North Pacific tropical cyclone activity *J. Clim.* **31** 5395–416
Patricola C M, Cassidy D J and Klotzbach P J 2022 Tropical oceanic influences on observed global tropical cyclone frequency *Geophys. Res. Lett.* **49** e2022GL099354
Rayner N A, Parker D E, Horton E B, Folland C K, Alexander L V, Rowell D P, Kent E C and Kaplan A 2003 Global analyses of sea surface temperature, sea ice, and night marine air temperature since the late nineteenth century *J. Geophys. Res.* **108** 4407
Sheng C, Zhang S, Liu Y, Wu G and He B 2023 Interannual impact of tropical southern Atlantic SST on surface air temperature over East Asia during boreal spring *Npj Climate and Atmospheric Science* **6** 186
Shi L, Zhan R, Zhao J and Kug J-S 2024 Mutating ENSO impact on Northwest Pacific tropical cyclones under global warming *Geophys. Res. Lett.* **51** e2023GL105864
Song J, Klotzbach P J and Duan Y 2022 On the relationship between western North Pacific tropical cyclone accumulated cyclone energy and the Pacific-North American pattern *Int. J. Climatol.* **42** 6373–83
Trenberth K E 1984 Some effects of finite sample size and persistence on meteorological statistics. Part I: autocorrelations *Mon. Weather Rev.* **112** 2359–68
Walsh K J E *et al* 2016 Tropical cyclones and climate change *Wiley Interdiscip. Rev. Clim. Change* **7** 65–89
Wang B and Zhou X 2008 Climate variation and prediction of rapid intensification in tropical cyclones in the western North Pacific *Meteorol. Atmos. Phys.* **99** 1–16
Wang C, Li C, Mu M and Duan W 2013 Seasonal modulations of different impacts of two types of ENSO events on tropical cyclone activity in the western North Pacific *Clim. Dyn.* **40** 2887–902
Wu B, Zhou T and Li T 2017a Atmospheric dynamic and thermodynamic processes driving the western North Pacific anomalous anticyclone during El Niño. Part I: maintenance mechanisms. *J. Clim.* **30** 9621–35
Wu B, Zhou T and Li T 2017b Atmospheric dynamic and thermodynamic processes driving the western North Pacific anomalous anticyclone during El Niño. Part II: formation processes. *J. Clim.* **30** 9637–50
Wang Q and Li J 2022 Feedback of tropical cyclones over the western North Pacific on La niña flavor. *Geophys. Res. Lett.* **49** e2021GL097210
Wu Y, Huang F, Xu S and Xing W 2020 Prediction of accumulated cyclone energy in tropical cyclone over the western North Pacific in autumn *Clim. Dyn.* **55** 3327–42
Wu T *et al* 2021 BCC-CSM2-HR: a high-resolution version of the Beijing climate center climate system model *Geoscientific Model Development* **14** 2977–3006
Yang Y, Zhu Z W, Shen X Y, Jiang L S and Li T M 2023 The Influences of Atlantic sea surface temperature anomalies on the ENSO-independent interannual variability of East Asian summer monsoon rainfall *J. Clim.* **36** 677–92
Zhan R, Wang Y and Lei X 2011 Contributions of ENSO and East Indian Ocean SSTA to the interannual variability of Northwest Pacific tropical cyclone frequency *J. Clim.* **24** 509–21
Zhan R and Wang Y 2016 CFSv2-based statistical prediction for seasonal accumulated cyclone energy (ACE) over the western North Pacific *J. Clim.* **29** 525–41
Zhang S, Liu Y, Sheng C and Ma T 2023 Influence of boreal spring sea surface temperature anomalies over the tropical South Atlantic on the Meiyu onset *Clim. Dyn.* **60** 3613–28
Zhao J, Zhan R, Murakami H, Wang Y, Xie S –P, Zhang L and Guo Y 2023 Atmospheric modes fiddling the simulated ENSO impact on tropical cyclone genesis over the Northwest Pacific *Npj Climate and Atmospheric Science* **6** 213